
Competitive folding of RNA structures at a termination–antitermination site

SORAYA AIT-BARA,^{1,2,3} CAROLINE CLERTÉ,^{1,2,3} NATHALIE DECLERCK,^{1,2,3,4} and EMMANUEL MARGEAT^{1,2,3}

¹CNRS UMR5048, Centre de Biochimie Structurale, 34090 Montpellier, France

²INSERM U1054, 34090 Montpellier, France

³Université de Montpellier, 34090 Montpellier, France

⁴INRA, département MICA, 78352 Jouy-en-Josas, France

ABSTRACT

Antitermination is a regulatory process based on the competitive folding of terminator–antiterminator structures that can form in the leader region of nascent transcripts. In the case of the *Bacillus subtilis* *licS* gene involved in β -glucosides utilization, the binding of the antitermination protein LicT to a short RNA hairpin (RAT) prevents the formation of an overlapping terminator and thereby allows transcription to proceed. Here, we monitored in vitro the competition between termination and antitermination by combining bulk and single-molecule fluorescence-based assays using labeled RNA oligonucleotide constructs of increasing length that mimic the progressive transcription of the terminator invading the antiterminator hairpin. Although high affinity binding is abolished as soon as the antiterminator basal stem is disrupted by the invading terminator, LicT can still bind and promote closing of the partially unfolded RAT hairpin. However, binding no longer occurs once the antiterminator structure has been disrupted by the full-length terminator. Based on these findings, we propose a kinetic competition model for the sequential events taking place at the termination–antitermination site, where LicT needs to capture its RAT target before completion of the terminator to remain tightly bound during RNAP pausing, before finally dissociating irreversibly from the elongated *licS* transcript.

Keywords: antitermination; transcription; fluorescence; single molecule; FRET

INTRODUCTION

Antitermination (attenuation) is a regulatory mechanism that prevents the premature termination of transcription to express needed genes otherwise silenced by an intrinsic terminator in their mRNA leader region (Gusarov and Nudler 1999). Intrinsic terminators are inverted repeats found on nascent RNA transcripts which fold into a stable hairpin structure immediately followed by a U-tract, a uridine-rich segment of 5–9 nucleotides (nt) (Fig. 1A). Transcription termination occurs when the RNA polymerase (RNAP) pauses at the U-tract where the Watson–Crick interactions in the RNA–DNA hybrid are weakened. Concomitant folding of the terminator hairpin leads to the release of the RNA and the disruption of the elongation complex (Naville and Gautheret 2010; Santangelo and Artsimovitch 2011). In the canonical mechanism of transcription antitermination, the formation of the terminator is compromised by the folding of an antiterminator RNA structure that partially overlaps and thus competes with the terminator (Naville and Gautheret 2010; Santangelo and Artsimovitch 2011).

This conformational switch between the terminator and antiterminator structures, usually mutually exclusive, can be controlled through diverse mechanisms, including temperature, translating ribosomes, or the binding of specific ligands such as metabolites, ions, uncharged tRNAs, or regulatory proteins (for review, see Smith et al. 2010; Santangelo and Artsimovitch 2011). Although many regulatory processes based on transcriptional antitermination have been described, especially in bacteria, the mechanistic and structural features that govern the differential folding of the nascent RNA and its functional consequences on the elongation complex are often poorly understood and seldom validated experimentally (Naville and Gautheret 2010; Santangelo and Artsimovitch 2011).

Antitermination proteins from the BglG/SacY family constitute an important family of factors involved in the regulation of sugar-metabolizing operons in both Gram-negative and Gram-positive bacteria (Mahadevan and Wright 1987; van Tilbeurgh and Declerck 2001; Amster-Choder 2005;

Corresponding authors: margeat@cbs.cnrs.fr, declerck@cbs.cnrs.fr
Article is online at <http://www.rnajournal.org/cgi/doi/10.1261/rna.060178.116>.

© 2017 Ait-Bara et al. This article is distributed exclusively by the RNA Society for the first 12 months after the full-issue publication date (see <http://rnajournal.cshlp.org/site/misc/terms.xhtml>). After 12 months, it is available under a Creative Commons License (Attribution-NonCommercial 4.0 International), as described at <http://creativecommons.org/licenses/by-nc/4.0/>.

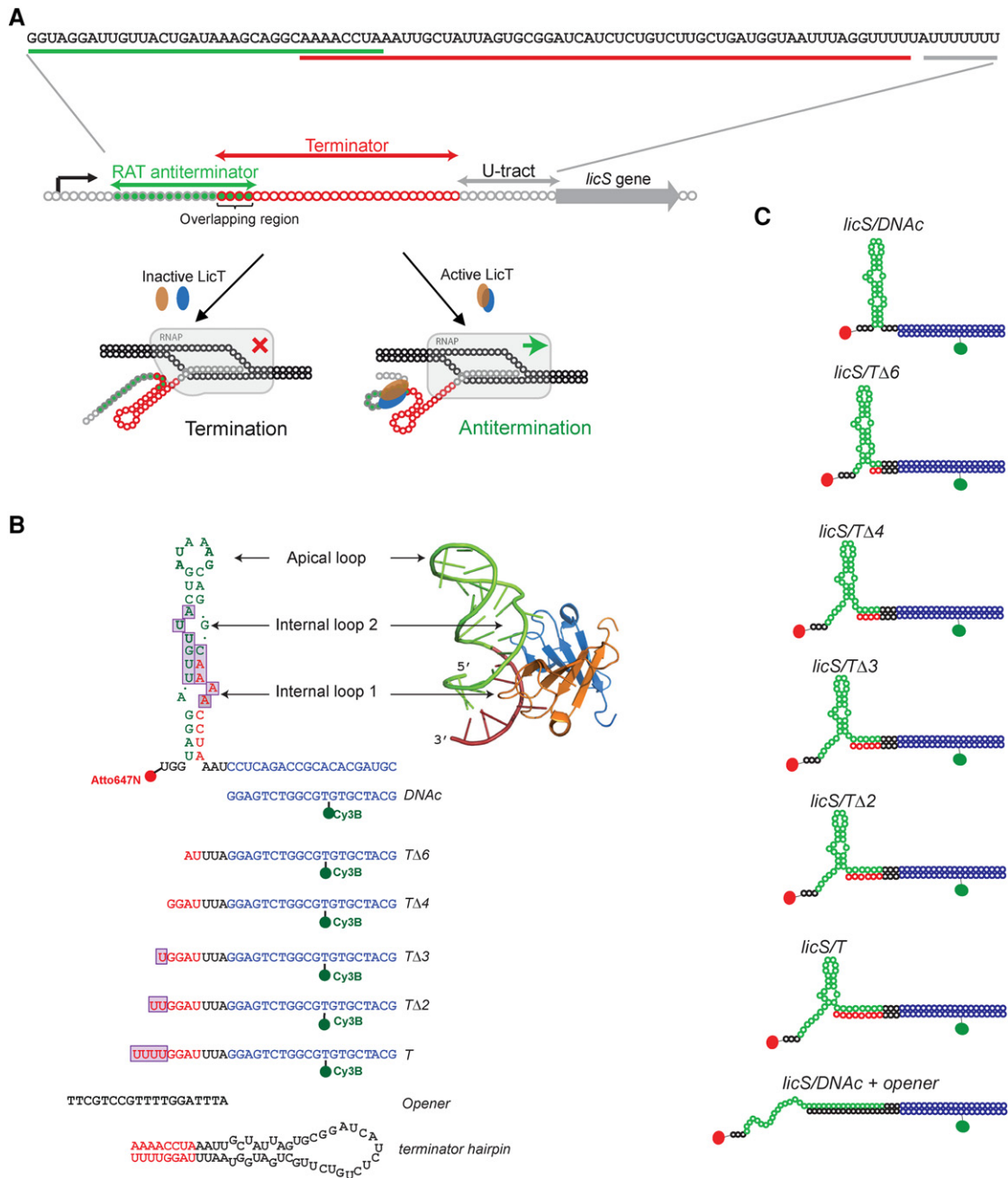


FIGURE 1. Antitermination mechanism and principle of the FRET-based assay used in this study. (A) Antitermination mechanism mediated by LicT and other antitermination proteins of the BglG/SacY family. The 5'UTR region of the *licS* gene contains a RAT antitermination sequence (green filled dots) and a terminator sequence (open red dots) followed by a U-tract. The RAT and terminator sequences are overlapping over 8 nt which make their folding into an RNA hairpin mutually exclusive. When LicT is inactive, the terminator sequence transcribed by the RNA polymerase folds into a strong hairpin that causes premature termination of transcription. Alternatively, the active LicT dimer binds and stabilizes the RAT hairpin to prevent the formation of the terminator and thereby allows transcription of the downstream *licS* gene coding sequence. (B) *licS* RNA hairpin, DNA and hybrid DNA/RNA oligonucleotides used in this study. The *licS* RNA is labeled at its 5' end with Atto647N. Nucleotides in red represent the 5' end of the terminator overlapping the 3' end of the *licS* RAT hairpin (in green). Nucleotides boxed in purple are involved in the interaction with the LicT-CAT dimer, as represented on the NMR structure of the LicT-CAT-RAT complex (Yang et al. 2002). (LicT-CAT monomer [orange and blue ribbons], RNA [green sticks + red sticks for the part overlapping with the terminator sequence]). This representation highlights the interaction of the orange monomer with loop 1, and the blue monomer with loop 2. An extension of 20 DNA nt (blue) is added at the 3' end of *licS* for hybridization with Cy3B-labeled DNA/RNA oligonucleotides of different lengths. These DNA/RNA hybrids mimic the 5' end of the terminator progressively invading the RAT antiterminator hairpin upon transcription by the elongating RNA polymerase. The DNA oligonucleotide *Opener* allows complete opening of the *licS* RNA hairpin. The terminator hairpin is represented, with the bases competing with the *licS* antiterminator highlighted in red. (C) Schematic of the *licS* RNA hybridized to Cy3B-labeled oligonucleotides and the *Opener*, showing the progressive opening of the *licS* RAT hairpin by the terminator mimics.

Joyet et al. 2013). *Bacillus subtilis* contains four of these anti-termination proteins, controlling the uptake and catabolism of sucrose (SacY and SacP), glucose (GlcT), and β -glucosides (LicT). These transcriptional regulators are characterized by an N-terminal RNA-binding domain (named *co*-antiterminator—CAT, about 55 residues) that interacts with a conserved RNA antiterminator (RAT) sequence overlapping an intrinsic terminator in the leader region of their specific target gene mRNAs (Fig. 1A; Aymerich and Steinmetz 1992). The C-terminal sensor region is made of two consecutive PTS regulation domains (PRD1 and PRD2) that are the sites of multiple phosphorylations by the phosphoenolpyruvate: sugar phosphotransferase system (PTS), the main sugar-transport system in bacteria (Stülke et al. 1998; Deutscher et al. 2006). PRDs are phosphorylated or dephosphorylated on conserved histidines by PTS proteins in response to the presence/absence of specific sugars, causing conformational changes that positively or negatively modulate the RNA-binding activity of the CAT domain (van Tilbeurgh and Declerck 2001; van Tilbeurgh et al. 2001).

LicT is orthologous to *Escherichia coli* BglG and is the best structurally characterized member of the BglG/SacY family. LicT regulates the expression of the *bglPH* operon encoding the β -glucoside-specific transporter BglP and the phospho- β -glucosidase BglH, and the *licS* (or *bglS*) gene encoding a β -glucanase (Krüger and Hecker 1995; Le Coq et al. 1995; Schnetz et al. 1996). When β -glucosides are absent, BglP inactivates LicT by phosphorylation of PRD1 whereas in the presence of a specific substrate, the phosphoryl groups of PRD1 are transferred back to BglP and subsequently to the incoming sugar. To be fully activated, LicT needs to be phosphorylated on PRD2 at both His207 and His269 by the PTS phospho-carrier protein HPr (Lindner et al. 1999; Tortosa et al. 2001). LicT activation by HPr-mediated phosphorylation occurs in the absence of glucose or other preferred carbohydrates but can also be induced constitutively by introducing a double His \rightarrow Asp mutation (H207D/H269D) mimicking phosphorylation of PRD2 (Tortosa et al. 2001; van Tilbeurgh et al. 2001). Structural studies have shown that LicT activation involves massive conformational changes that stabilize the LicT dimer and trigger a helix-coil transition in the linker region connecting the PRDs to the CAT RNA-binding domain (Declerck et al. 2001; van Tilbeurgh et al. 2001; Graille et al. 2005; Déméné et al. 2008). In the activated form, the CAT dimer interacts with high affinity and specificity to the antiterminator RAT sequence found in the 5' untranslated region (UTR) of the *bglH* and *licS* genes (Declerck et al. 1999, 2001). NMR studies have revealed how both monomers of CAT interact with similar structural elements of the RAT hairpin in the LicT/*licS*-RNA antitermination complex (Fig. 1B; Yang et al. 2002).

The canonical RAT sequence recognized by BglG/SacY antitermination proteins is a 29- to 33-nt long RNA segment sharing 6–10 nt at the 3' end with the 5' end of an intrinsic terminator sequence (Manival et al. 1997; Clerte et al. 2013).

All RAT sequences are predicted to fold into a hairpin with an apical loop of variable length and sequence, and a double-stranded stem interrupted by two highly conserved internal loops that constitute the main recognition feature for the binding of the CAT dimer (Aymerich and Steinmetz 1992). Nucleotides that are important for the structural maintenance of the RAT hairpin, as well as residues that constitute specificity determinants for CAT/RAT recognition have been determined by site-directed mutagenesis and NMR (Fig. 1B; Aymerich and Steinmetz 1992; Declerck et al. 2002; Hübner et al. 2011). Recently the length of the stem formed at the base of *licS*-RAT (targeted by LicT) and *sacB*-RAT (targeted by SacY) has also been shown to be crucial for the stability of the antiterminator hairpins and their recognition by their cognate antitermination protein (Clerte et al. 2013). Formation of the intrinsic terminator being thermodynamically favored, the RAT hairpin needs to be stabilized by the bound antitermination protein in order to resist the competitive folding of the terminator hairpin. Stabilization of RAT in double-stranded conformation has indeed been observed in vitro upon addition of antitermination proteins (Manival et al. 1997; Yang et al. 2002; Himmel et al. 2012).

In spite of numerous studies that have shed light on the antitermination mechanism mediated by BglG/SacY-like proteins, there are still many open questions regarding the sequence of events that orchestrate this regulatory process at the termination-antitermination sites and determine the fate of transcription. What is the structure and dynamics of the RNA molecules, and how are they balancing between alternative conformations upon elongation of the RNA transcript by the RNAP, or upon binding of the antitermination protein? Is the antitermination protein able to bind to the partially folded hairpin while the RAT sequence is being transcribed? How strongly and how long does the antitermination protein need to bind in order to prevent disruption of the RAT hairpin by the invading terminator during transcription and subsequent pausing of the RNAP? Can the antitermination protein recognize and/or refold a partially or completely disrupted RAT hairpin? Does the antitermination protein remain bound to its mRNA target after the RNAP has escaped the termination site?

We have started to address some of these questions using single-molecule Förster resonance energy transfer (smFRET). This technique enables the study of biomolecular dynamics, interactions, and multiple conformations that are undetectable by bulk biochemical methods or conventional structural and atomic-level approaches (Weiss 2000). Recently, we developed a fluorescence-based nucleic acid system that mimics the competitive folding of antiterminator-terminator hairpins and used smFRET to monitor directly the opening and closing state of RAT hairpins in the presence of terminator-mimicking oligonucleotides and/or antitermination proteins (Clerte et al. 2013; Ait-bara et al. 2015). In this initial work, we showed for *licS*-RAT and *sacB*-RAT derived RNAs

that the antiterminator hairpins adopt spontaneously a closed structure and that antitermination protein binding can efficiently counteract the competing binding of a terminator mimic DNA oligonucleotide. In the present study, we have refined our experimental scheme in order to investigate the effect of the progressive transcription of the terminator sequence on the *licS*-RAT open/closed equilibrium and on LicT binding/stabilizing ability. A series of fluorescent RNA oligonucleotidic constructs was designed to mimic the competing terminator that progressively invades the RAT antiterminator hairpin upon transcription by the RNA polymerase. We quantified by bulk fluorescence anisotropy measurements the interaction of LicT with these constructs and found that the high affinity of binding is drastically altered as soon as the short basal stem of the RAT hairpin is disrupted. We then used smFRET combined with a pulsed interleaved excitation (PIE) configuration that enables accurate measurements of fluorescence parameters such as FRET efficiency and fluorescence lifetimes of freely diffusing biomolecules diluted at picomolar concentrations (Hendrix and Lamb 2013; Olofsson and Margeat 2013). These measurements revealed multiple conformational states of the *licS*-RAT hairpin, becoming more and more open upon competition by terminator mimics of increasing length. We found that LicT can still recognize and promote the closed state of the partially melted RAT hairpins, and that it is only once the antiterminator structure has been completely disrupted by the full-length terminator mimic that the stabilizing effect of LicT is abolished. Simulation of the *licS* RNA cotranscriptional folding pathway further supports conclusions from our experimental data. Altogether our results bring new insight on several aspects of the LicT-mediated antitermination mechanism, in particular the necessity for the antitermination protein to capture its RNA target before the terminator is fully transcribed and to remain tightly bound to it during the time the RNAP is pausing at the U-tract. Based on these and previous findings, we propose a kinetic model of the LicT-regulated competitive RNA folding process taking place at the termination–antitermination site of transcription.

RESULTS

An experimental design to mimic the terminator–antiterminator competition

In order to investigate the folding/unfolding kinetics of the competing antiterminator–terminator hairpins during transcription, we refined the experimental set-up that we previously designed for monitoring the opening and closure of the RAT hairpin by smFRET (Clerte et al. 2013). In the 5'UTR of the *licS* mRNA targeted by LicT, the 3' end of the *licS*-RAT sequence overlaps by 8 nt the 5' end of an intrinsic terminator (Fig. 1A). When the 3' end of the terminator sequence is being transcribed, it competes with *licS*-RAT for these shared nucleotides to complete the basal stem of the

terminator hairpin, thereby disrupting the antiterminator hairpin. In order to monitor the conformational changes undergone by the RAT hairpin during this process, we used an RNA oligonucleotide corresponding to the natural 33-nt long *licS*-RAT sequence recognized by LicT, and labeled with Atto647N at its 5' end (Fig. 1B). At the 3' end, an artificial DNA extension of 20 nt was added in order to hybridize a Cy3B-labeled complementary strand (Fig. 1B). The position of Cy3B (donor) relative to Atto647N (acceptor) at the *licS* RNA 3' end had been previously optimized in order to maximize the changes in the FRET signal reporting for the spatial proximity between the two fluorescent probes (Clerte et al. 2013). In our previous study, we had used short DNA oligonucleotides of weak affinity, complementary to the RAT basal stem to mimic the competing terminator. Here we used RNA/DNA chimeric oligonucleotides, composed of a 20-nt-long DNA sequence (*DNAc*) that hybridizes efficiently with the 3' end extension of the Atto647N-*licS* construct (Fig. 1B, blue nucleotides), fused to a 3' RNA part of increasing length (Fig. 1B, black/red nucleotides). When present, this 3'RNA part corresponds to the 3' end of the terminator fully transcribed (referred as T) or partially transcribed (referred as T Δ 2 to T Δ 6) (Fig. 1B). The RNA segment of these DNA–RNA chimeras can hybridize with the last 2 (T Δ 6), 4 (T Δ 4), 5 (T Δ 3), 6 (T Δ 2), or 8 (T) nt of the *licS*-RAT sequence, and therefore mimic the terminator that progressively invades the antiterminator upon processive transcription by RNAP (Fig. 1B,C; Supplemental Fig. 1A). When compared to our initial work (Clerte et al. 2013; Ait-bara et al. 2015), this new experimental design presents two advantages: First, the competing oligonucleotides mimicking the terminator being transcribed can be strongly hybridized to the *licS*-RNA construct, owing to a long complementary sequence that ensures the stability of the hybrids; second, the terminator 3' end is now made of RNA instead of DNA, and thus better represents the natural situation.

We first used fluorescence gel mobility shift assay (F-EMSA) to check our different RNA/DNA hybrids and to determine whether they can be efficiently recognized by the antitermination protein LicT (Fig. 2A; Supplemental Fig. 1C). We used the purified full-length and activated mutant LicT protein (LicT*) that was previously shown to constitutively activate expression of the *licS* gene in vivo (Tortosa et al. 2001) and to bind with high affinity and specificity to *licS*-derived RNAs in vitro (Declerck et al. 1999; van Tilbeurgh et al. 2001; Clerte et al. 2013). LicT* at 1 μ M results in a shift in the migration of both *licS* alone and the *licS*/*DNAc* hybrid, indicating that the hybridization of *DNAc* to the 3' end of *licS* does not hamper the binding of LicT*, as previously shown (Clerte et al. 2013). In contrast, no band shift was observed for the *licS*/T hybrid mimicking the fully transcribed terminator, consistent with LicT* binding being completely abolished upon formation of the full-length terminator that disrupts the structure of the RAT hairpin. Interestingly, a gradual decrease of the shifted band intensity was observed

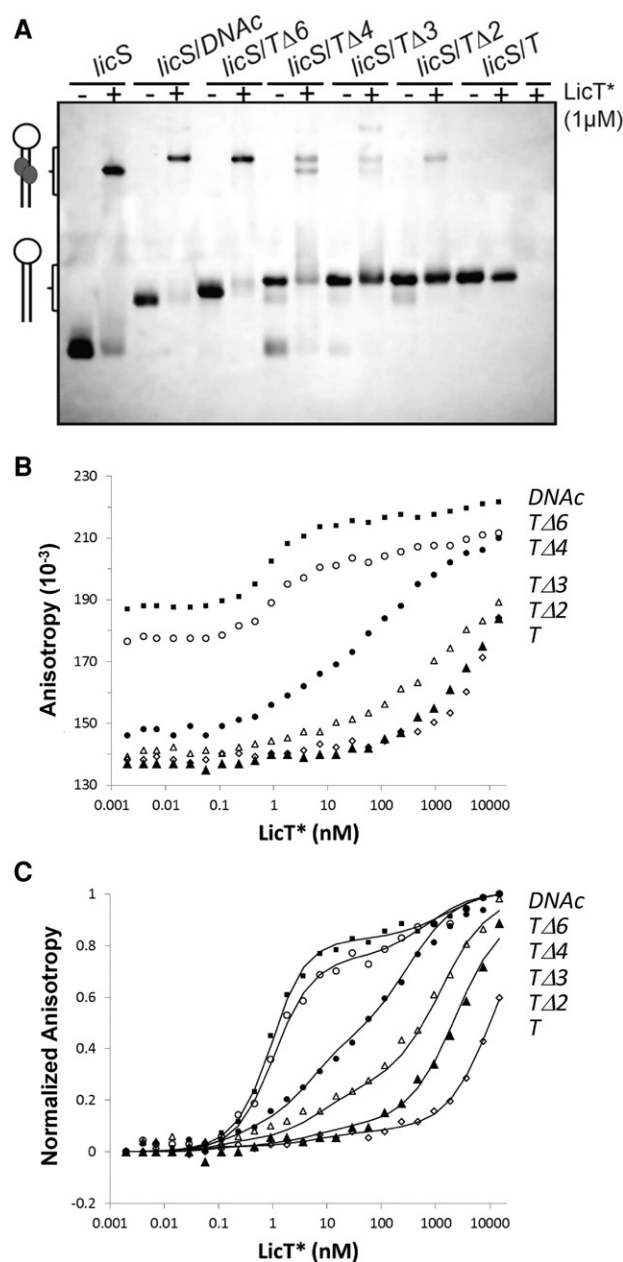


FIGURE 2. Effect of terminator mimics on the binding of activated mutant LicT* to different RNA hybrids. (A) Gel mobility shift assay with LicT* (1 μM) and Atto647N-*licS* RNA alone (1 nM) or with different RNA hybrids (500 nM). (B) Raw fluorescence anisotropy binding profiles with different RNA hybrids (0.4 nM) at 150 mM NaCl by LicT* ([black square] *licS/DNAc*; [open circle] *licS/TΔ6*; [black circle] *licS/TΔ4*; [open triangle] *licS/TΔ3*; [black triangle] *licS/TΔ2*; [open diamond] *licS/T*). (C) Fluorescence anisotropy binding profiles normalized from the plateau of the low affinity binding at saturating concentration, recovered from the fit. Data were fitted using a double-binding model of high affinity (~nM) and low affinity (~μM) (see main text).

with the *licS/TΔn* hybrids corresponding to the partially transcribed terminator: LicT* binding does not seem to be affected by the hybridization of *licS* to *TΔ6* (missing the last 6 nt of the terminator), whereas it decreases rapidly with the

increase of length of the terminator mimics (*TΔ4*, *TΔ3*, and *TΔ2*). These results indicate that, as expected, the interaction of LicT* with the antiterminator hairpin is gradually reduced upon competition with RNA sequences corresponding to the progressively transcribed terminator, validating our experimental design.

Loss of LicT* high affinity binding to RNA upon terminator completion

The interaction of LicT* with the RNA/DNA hybrids was then quantitatively monitored by fluorescence anisotropy binding assays (Heyduk et al. 1996; Clerte et al. 2013). Figure 2B shows the binding profiles of LicT* to the 5' Atto647N-labeled *licS* RNA hybridized to the different oligonucleotides used in Figure 2A. It can first be noted that the anisotropy value of the free hybrids measured at the lowest (picomolar) protein concentration (i.e., in the absence of bound protein) decreased rapidly with the increase in length of the competing terminator sequence. Since the molecular weight of these constructs increases with the length of the sequence, an increase in anisotropy would have been expected. This observed decrease reflects instead a gain in local mobility of the RNA fragment bearing the fluorophore, in good accordance with the 5' end of the RAT hairpin becoming more and more flexible upon its disruption by the invading terminator. As expected, for all constructs, the anisotropy values increased upon addition of increasing concentration of LicT*, but a very important decrease of LicT* apparent affinity for RNA was observed as the terminator length increased. The titration data were fitted using a double-binding model of high affinity (~nM) and low affinity (~μM). This model could represent either a specific binding of LicT to its target, followed by nonspecific binding of additional LicT molecules, or, more probably (see below) the high affinity binding of LicT to a population of properly folded antitermination hairpins, together with the low affinity binding of LicT to partially disrupted antitermination hairpins.

For *licS* hybridized to DNAc (containing no competing terminator RNA sequence) the high affinity K_d value of 0.65 ± 0.02 nM (Supplemental Table S1) is similar to the binding affinity constant determined previously for the binding of *licS* alone (Clerte et al. 2013). This very high affinity binding was completely abolished upon addition of 5 μM *opener*, a DNA oligonucleotide that opens and disrupts entirely the *licS* RNA hairpin by hybridizing up to the apical loop (Supplemental Fig. S2), demonstrating the absence of nonspecific protein/nucleic acid interactions under the assay conditions we used (150 mM NaCl, pH 8). LicT* binding to its intact *licS* target remained practically unchanged in the case of the *licS/TΔ6* hybrid containing the shortest terminator sequence which can displace only 2 nt of the RAT hairpin at the base of the stem. In contrast, a severe effect was observed with *licS/TΔ4* containing an additional 2 nt at the 3' end of the terminator mimic. This latter competes for

the entire basal stem of the *licS* hairpin and thereby can disrupt internal loop 1, leaving only internal loop 2 available for LicT* binding. This disruptive effect became more and more pronounced when the terminator sequence became more and more complete, as seen with the *licS/TA3*, *licS/TA2* and *licS/T* hybrids. For these hybrids the titration curves spread over a very large range of protein concentration, not compatible with a simple interaction model considering only a single site or RNA species for the binding of the LicT* protein. Instead, a proper fit was obtained using a binding model for which a high affinity interaction event would first take place in the nanomolar range of protein concentration, followed by a low affinity interaction event taking place in the micromolar range and that would dominate upon disruption of the *licS*-RAT hairpin by the invading terminator (see fits on Fig. 2C; Supplemental Table S1). Note that this thermodynamic model based on bulk fluorescence measurements cannot distinguish between two independent conformational states of the RNA or two binding sites coexisting in the RNA probe. From the normalized curves representation shown in Figure 2C, it appears that the fraction of probe available for high affinity binding decreases upon increasing the length of the terminator mimic. This would be consistent with a model where properly folded antiterminator hairpins, where high affinity binding occurs, coexist with partially unfolded ones. Thus, we next used single-molecule FRET experiments to verify and further validate this hypothesis.

RNA multiple conformations revealed by smFRET

To investigate the structure and conformational changes of the *licS* RNA hairpin at the single-molecule level, we performed smFRET experiments on the doubly labeled constructs described above, using a homemade confocal microscope with a pulsed interleaved excitation (PIE) configuration (Olofsson and Margeat 2013). smFRET enables studying molecular interactions of freely diffusing biomolecules diluted at picomolar concentrations, by accurate measurements of fluorescence parameters such as FRET efficiency and fluorophores excited-state lifetimes. Here, we used the energy transfer that occurs between Cy3B (donor) and Atto647N (acceptor) fluorophores as a reporter of the spatial proximity between the two dyes, to inform us about the structural conformation of the RAT hairpin competed with terminator mimics. It is expected that the invasion of the *licS* RNA hairpin by terminator mimics will progressively unfold the hairpin and thereby increase the distance between the two fluorophores (Fig. 1C). Since the FRET efficiency, related to this distance, is measured at the single-molecule level, any heterogeneity of the hairpins in terms of conformation will be directly assessed.

In the case of the *licS/DNAc* hybrid (Fig. 3A, left panel), we observed a single peak of high apparent energy transfer values, with an average proximity ratio (E_{PR}) of 0.72, indicating

the presence of a homogeneous population of RNA molecules in which the two dyes are in close proximity. This population corresponds to the closed state of the fully folded RNA hairpin in solution as previously shown (Clerte et al. 2013). In the case of the *licS/TA6* construct, a single peak is also recovered but with a significant decrease of the apparent FRET efficiency (mean E_{PR} value dropping from 0.72 to 0.53, Fig. 3B, left panel). This decrease can be at least partly explained by the increase of the distance between the dyes due to the presence of three additional base pairs that mimic the basal stem of the terminator before it starts to invade the RAT hairpin (UAA, Fig. 1B, black nucleotides). In addition, a slightly wider distribution is observed, suggesting rapid equilibrium between different closed states of the *licS* hairpin, invaded or not by the two competing nucleotides in its basal region (AU, Fig. 1B, red nucleotides). This observation was confirmed by the analysis of the excited-state lifetime of the donor fluorophore within these doubly labeled molecules. Indeed, while a single exponential decay was sufficient to describe these data in the case of the *licS/DNAc* hybrid, the proper description of *licS/TA6* data required a double exponential function, indicating the presence of at least two (or a distribution of) distances (Supplemental Fig. S3).

In contrast, a clear bi-modal distribution of E_{PR} values was observed with the *licS/TA4* hybrid, indicative of the coexistence of alternate RNA conformations being in slow equilibrium (slower than the diffusion time of the labeled molecules in the observation volume, i.e., a few milliseconds), and therefore detectable as distinct populations in the E_{PR} histograms (Fig. 3C, left panel). Multiple Gaussian fitting of the histogram using the program Origin (OriginLab) proposed the presence of a minor population with a high apparent FRET efficiency ($E_{PR} = 0.65$) consistent with a closed *licS* hairpin, as observed in the absence of competitor, and a major population displaying an intermediate energy transfer value ($E_{PR} = 0.46$) that could correspond to the partially unfolded RAT hairpin retaining only one internal loop (loop 2). A similar equilibrium is also observed in the smFRET data recovered with the *licS/TA3* and *licS/TA2* hybrids for which a very low but visible contribution of the closed, high-energy transfer state was still observed along with a major peak of intermediate value ($E_{PR} \sim 0.40$) comprising over 90% of the RNA molecules (Fig. 3D,E, left panels).

Finally with the full-length terminator mimic *licS/T*, we obtained a predominant peak of low FRET value ($E_{PR} = 0.30$) that likely emanates from completely unfolded conformation(s) of the *licS* RNA, together with a minor peak of intermediate E_{PR} value contributing to $\sim 20\%$ of the total RNA molecules and that could correspond to the partially unfolded hairpin as seen with the terminator mimics lacking 2, 3, or 4 nt (Fig. 3F, left panels). However, in the case of the full-length terminator, no molecule with a high E_{PR} value was detected, indicating that no detectable folded RAT hairpin remains in the population.

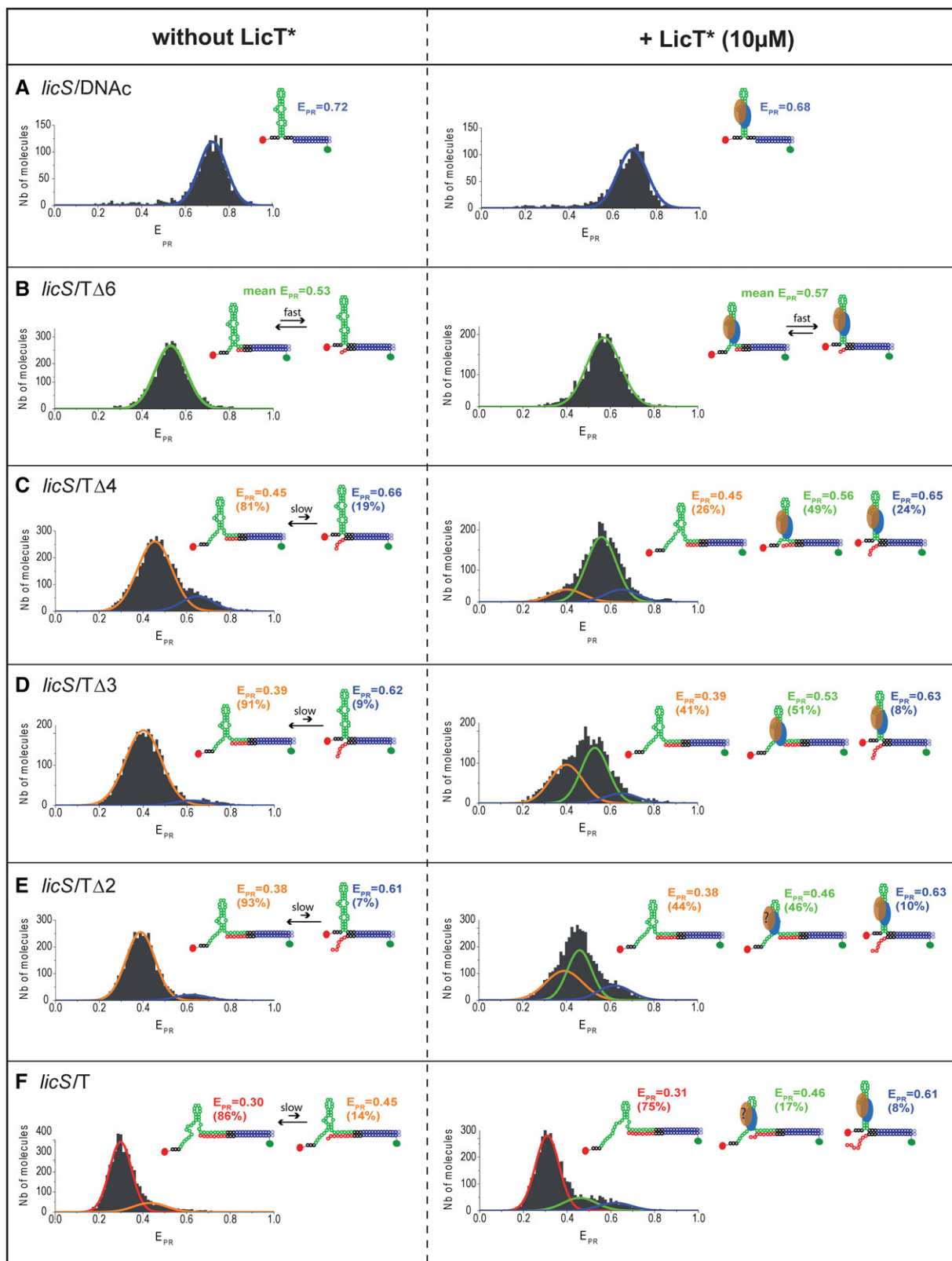


FIGURE 3. Effect of terminator mimics on LicT* binding to RNA hybrids monitored by smFRET-PIE experiments. (A–F) Distribution of apparent FRET efficiencies (E_{PR}) in the population of RNA molecules (10 pM) are determined at 150 mM NaCl in the absence (left panels) or in the presence (right panels) of active LicT* (10 µM). For each panel, the observed distributions are deconvoluted into populations containing partially or totally folded RAT hairpins (see text). For each subpopulation, the indicated E_{PR} value and fractional population is the mean value obtained from two or three experiments (see Supplemental Table S2).

LicT*-dependent stabilization of the RAT hairpin

In order to monitor the effect of the antitermination protein on the *licS*-RAT hairpin competed with the terminator mimics, we repeated our experiments in the presence of LicT* at 10 μ M (Fig. 3, right panels). At this concentration, the activated form of LicT is expected to be a dimer in solution (Declerck et al. 2001) and to bind at saturation the *licS*-RNA if properly folded (Fig. 2B). In the case of the *licS/DNAc* hybrid with no competing RNA sequence, addition of LicT* leads to an unexpected slight decrease in the FRET efficiency compared to that in the absence of protein (mean E_{PR} value decreasing from 0.72 to 0.69, Fig. 3A). By selecting donor-only or acceptor-only molecules, we verified that this small but reproducible effect was not due to LicT* influencing the fluorescence lifetime of the fluorophores and their count rate, or emission anisotropy (data not shown). It can thus be concluded that the decrease in FRET efficiency observed upon LicT* binding resulted from an increase of the distance between the two fluorophores, indicating that the closed state of the *licS* hairpin is slightly different in the free RNA and in the complex formed with the antitermination protein.

Inversely, we noticed a slight increase of the mean E_{PR} value measured for the *licS/T Δ 6* hybrid molecules upon addition of LicT* (from 0.53 to 0.57, Fig. 3B, with a wide distribution as observed in the absence of protein). Thus, as in the case of the *licS/T Δ 6* alone, we propose that the *licS*-RAT hairpin would be in rapid equilibrium between at least two slightly different closed states, the binding of the antitermination protein favoring the one excluding the 2 nt of the *T Δ 6* terminator mimic competing for the basal stem. Addition of LicT* to the *licS/T Δ 4*, */T Δ 3*, or */T Δ 2* hybrids caused an even more important shift of the peaks toward higher E_{PR} values, in agreement with an overall stabilization of *licS*-RNA closed conformations. However, a high conformational heterogeneity remains in the population of RNA molecules, as revealed by the wide and complex distributions of smFRET values observed. Based on the deconvolution performed for the RNA constructs alone (Fig. 3C–E, left panels), we fitted the data by considering an additional species, representing a partially folded hairpin in the protein bound state ($E_{PR} = 0.46$ – 0.56). The fact that the binding of LicT* to the partially folded hairpin increases the spatial proximity of the two dyes suggests that the antitermination protein promotes further but still incomplete closing of the RNA molecules. Interestingly, with the full-length terminator *licS/T* a significant fraction ($25 \pm 2\%$) of the RNA molecules could also be detected in the protein bound state. However, as in the case of *licS/T Δ 2*, only a very small fraction ($8 \pm 2\%$ and $10 \pm 3\%$, respectively) is observed in the high energy transfer state corresponding to the complex where the RAT hairpin has both internal loop 1 and 2 properly folded (Fig. 3F, right panels).

Very similar smFRET distributions and deconvolved data were obtained for three sets of independent experiments per-

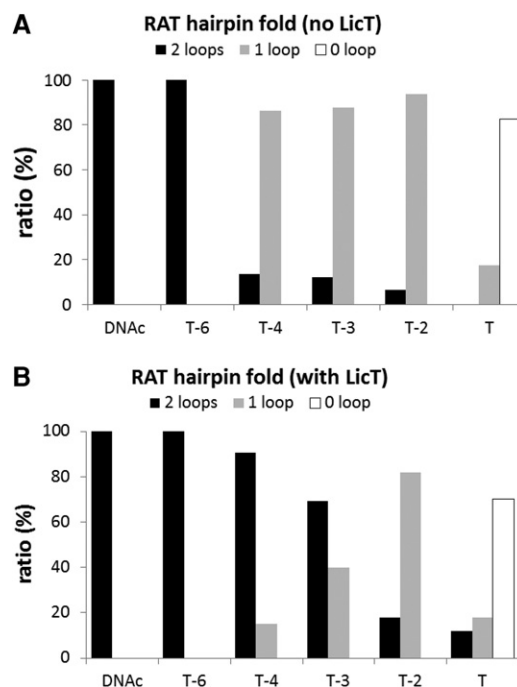


FIGURE 4. Percentage of antiterminators hairpins in a state where 0 (white), 1 (gray), or 2 (black) internal loops are properly folded, in the absence (A) or presence (B) of 10 μ M LicT*. Values were calculated from the deconvolved smFRET data obtained from three independent data sets similar to the one presented in Figure 3, with mean and standard error of the mean (SEM) values reported in Supplemental Table S2. The effect of LicT on the folding of both loops in the RAT hairpin is clearly seen for *licS/T Δ 4* and *licS/T Δ 3*.

formed under identical conditions in the presence or absence of LicT* (Fig. 4; Supplemental Table S2). Based on their E_{PR} value, RNA species were assigned to a different fold of the RAT sequence: a closed hairpin exhibiting both LicT recognition loops 1 and 2 ($E_{PR} > 0.50$), a partially open hairpin with only the loop 2 properly folded ($0.50 > E_{PR} > 0.34$), or an unfolded conformation with no recognition loop ($E_{PR} < 0.34$) (Fig. 4A,B). According to this analysis, LicT binding clearly favors closed conformations of the *licS* RNA molecules, thereby counteracting the opening of the RAT hairpin upon invasion by the terminator. However, in the cases where the terminator is almost fully transcribed (*licS/T Δ 2* and *licS/T*), LicT binding cannot promote the proper folding of the recognition loop 1, that is required to counteract the hybridization of the terminator stem.

Simulation of *licS*-RNA cotranscriptional folding pathway

We sought to determine whether a simulation of the RNA folding during the transcription of the antiterminator–terminator sequence could reproduce the sequence of events that were identified at equilibrium in our smFRET assays. We have used the *kinfold* server that calculates and animates

RNA folding paths (Xayaphoummine et al. 2005) to simulate the kinetics of folding/unfolding of the RNA sequence corresponding to the 5'UTR region of the natural *licS* mRNA while being transcribed. Although generated automatically using default parameter values, the predicted scenario of termination reproduces remarkably well the one proposed based on our experimental data. As seen in the first simulation (Supplemental Movie S1), nucleation of the RAT hairpin initiates as soon as the nucleotides forming the apical stem-loop emerge from the elongation complex. Internal loop 2 is then readily formed after synthesis and pairing of the nucleotides of the central stem. Formation of recognition loop 1 is governed by hairpin closure accompanying base-pairing between the 5' and 3' ends of the RAT sequence once complete, in good accordance with a previous finding that the *licS*-RAT RNA adopts spontaneously the closed structure of a functional antiterminator (Clerte et al. 2013). The RAT hairpin then remains stably closed until the 3' end of the terminator sequence starts to compete for duplex formation at the RAT basal stem, disrupting recognition loop 1 then loop 2, until completion of the full terminator hairpin. In the simulation, disruption of loop 1 occurs when the terminator still lacks 5 nt whereas it is only when the terminator sequence is fully transcribed that it can disrupt loop 2. This is in very good agreement with our smFRET data using terminator mimics of increasing length, indicating that the RAT hairpin is preserved in the presence of *TΔ6*, retains only loop 2 when competed by *TΔ4* and *TΔ3*, and is essentially unfolded when invaded by the full-length terminator sequence (Fig. 3, left panels).

Finally, in order to simulate the stabilization of the RAT hairpin through the binding of the antitermination protein, we have forced base-pairing in the RAT basal stem during synthesis and folding of the terminator hairpin (Supplemental Movie S2). Stabilization of the three base pairs following loop 1 prevents the displacement of the RAT 3' end, and thus precludes the completion of the termination hairpin. According to this simulation, the free energy of the final *licS* RNA structure in the antitermination scenario is 6.6 kcal mol⁻¹ higher than that of the freely folded RNA structure harboring the full terminator hairpin. This would represent the minimal energetic cost for the maintenance of the *licS*-RAT hairpin that should be compensated by LicT binding, in order to achieve antitermination.

DISCUSSION

Although transcription antitermination by BglG/SacY-like proteins was first described over 30 yr ago (Steinmetz and Aymerich 1986; Mahadevan and Wright 1987) and has been the subject of intensive studies since then, there are still many aspects of the molecular mechanism by which these proteins perform their regulatory task that remain elusive in the absence of experimental evidence. Although non-canonical RAT sequences that are not necessarily associated

with terminators and whose function remains unclear have been identified (Tortosa and Le Coq 1995; Daguer et al. 2004; Gordon et al. 2015), the general mechanism of regulation mediated by BglG/SacY proteins relies on the competition between mutually exclusive RNA terminator–antiterminator structures. The development of single-molecule fluorescence-based methods have recently opened the way to new fields of investigation, in particular regarding critical aspects of the structure and dynamics of the short RNA hairpins targeted by these antitermination proteins, on which little is still known. In the present work, we studied the binding of LicT to its cognate *licS*-RAT hairpin using a combination of fluorescence anisotropy and single-molecule FRET experiments. We used the constitutively active protein LicT* and doubly labeled oligonucleotidic constructs designed to mimic the folding state of the antiterminator hairpin progressively invaded by the terminator sequence during transcription by the RNAP. Our experimental design is greatly simplified compared to the *in vivo* situation where the actual formation of RNA secondary structure is strongly influenced by the presence of the elongation complex and accessory factors, and where the 3' end of the transcript is engaged in the RNA:DNA hybrid. However, at the RNA level, this minimal system allows us to investigate from an equilibrium point-of-view the structural features associated with this termination–antitermination competition.

Our results of fluorescence anisotropy measurements show that the strong interaction of LicT with the *licS* RNA is abolished as soon as the internal loop 1 of the antiterminator hairpin is disrupted upon competition by the terminator 3' end. This loop, together with the other internal loop 2 (Fig. 1A), constitute the main recognition features for the binding of the LicT dimer. Moreover, it is the only one partially overlapping with the terminator stem (Fig. 1B). Thus, its proper folding and stability constitute probably key elements in the process of termination–antitermination balance. The 3D structure of the LicT-CAT RNA-binding domain solved by NMR in complex with the *licS* RAT hairpin has revealed in detail how each monomer of the homodimer interacts in a very similar way with these two structurally equivalent internal loops (Fig. 1B; Yang et al. 2002). Any modification that alters the structure or stability of these loops is thus expected to reduce the RNA-binding affinity of the antitermination protein. Interestingly, we found that the anisotropy titration curves recovered for *licS* hybridized to terminator mimics of increasing length could be properly fitted when considering two binding events, one in the nanomolar range as observed in the absence of RNA competitor, and the other in the micromolar range or above (Fig. 2C). Such binding behavior could be explained by the presence of either two different binding sites on the target RNA, or two different populations of the RNA molecules being in a high or low affinity conformational state. Although our results of FRET experiments at the single-molecule level clearly favor this second interpretation (see below), we cannot exclude an interaction

model in which the binding of the LicT* dimer to partially folded RAT hairpins involves two steps where one monomer first associates with high affinity to the preserved internal loop 2, and the second monomer next interacts with low affinity to the misfolded recognition loop 1. Given the known dimeric structure of the LicT–CAT domain in complex with *licS*-RAT (Fig. 1B; Yang et al. 2002), it seems, however, highly unlikely that a single CAT monomer could form a high affinity complex with RNA. Nevertheless, this possibility cannot be totally ruled out in the absence of kinetic binding studies on LicT/RNA interaction, therefore the eventual binding of monomeric LicT to partial or full antiterminator hairpins remains an open question.

The complex, multimodal histograms recovered by smFRET reflect the high structural heterogeneity among the population of molecules being observed. This was particularly the case for the RNA probes mimicking the partially transcribed terminator, supporting our model where the *licS*-RAT in these constructs adopts multiple conformations that are differently recognized by LicT*. Deconvolution of our smFRET data suggests the coexistence of several RNA species in which the *licS*-RAT hairpin contains zero, one, or two internal loops properly folded (Figs 3, 4; Supplemental Table S2). The RNA molecules folded with two loops would constitute the high affinity species, a structure that, when formed, competes with the complete folding of the terminator; those with only one loop (presumably loop 2) the species that can be bound by the antitermination protein at low affinity, leading to a further folding of the antiterminator structure; finally, the RNA molecules with no loop that could not be bound by the antitermination protein. The relative contribution of each RNA species to the total population would depend on both the length of the terminator mimics and the binding efficiency of the antitermination protein. Consistent with this model, in the normalized binding curves recovered with the different RNA probes (Fig. 2C), the value of the intermediate plateau reflecting the abundance of RNA molecules in the high affinity state bound by LicT* is in rather good accordance with the proportion of RNA molecules detected in the high FRET state corresponding to the closed RAT hairpin (Fig. 3, left panels). The relative anisotropy values reached at the end of the titration (at 15 μ M of LicT*, Fig. 2C) are also in good accordance with the fraction of bound RNA molecules detected by smFRET in the presence of LicT* added at 10 μ M (Fig. 3, right panels).

An important finding of this study is that, although the high affinity binding of LicT* for RNA is rapidly compromised upon invasion of the RAT hairpin by the terminator sequence, the antitermination protein can still interact specifically with the *licS* RNA as long as it presents residual structural elements of the antiterminator hairpin. This was demonstrated by both anisotropy binding and smFRET experiments with the *T Δ 4*, *T Δ 3*, and *T Δ 2* competitor RNA that can disrupt internal loop 1 but preserve the apical loop and internal loop 2 of the RAT hairpin (Fig. 1B). Over

80% of the *licS*-RNA molecules hybridized to these terminator mimics was detected in an intermediate open state attributed to the partially unfolded RAT hairpin retaining only internal loop 2 (Fig. 3C,D, left panels; Fig. 4). Nevertheless, specific binding of LicT* to these hybrids still occurs at sub-micromolar protein concentration (Fig. 2C), which is not the case when the RAT hairpin is completely destructured (either by competition with the *Opener* oligonucleotide [Supplemental Fig. S2], or in the presence of the full terminator mimic [*licS/T*]). Moreover, our smFRET experiments indicate that after addition of LicT* at 10 μ M, over 80% of the *licS/T Δ 4* hybrids and 60% of the *licS/T Δ 3* hybrids are detected in a protein-bound state where the RAT hairpin is almost fully closed (Fig. 3D,E, right panels). This implies that the antitermination protein is able not only to recognize the RAT hairpin with just internal loop 2, but also to promote the refolding and stabilization of internal loop 1, counteracting its disruption by the partially transcribed terminator sequence. This implies also that, during transcription of the *licS* mRNA leader region, LicT binding can occur as soon as the minimal recognition features of the RAT hairpin are formed, i.e., the apical loop and internal loop 2; then the antitermination protein, even weakly bound, can assist the folding of the remaining antiterminator sequence once transcribed in order to form a high affinity protein–RNA complex that can resist to the invading terminator. However, if LicT* is not bound upon transcription of the full-length terminator sequence, the *licS*-RNA molecules adopt a destructured conformation that can no longer be recognized by the antitermination protein (Fig. 3F). The functional implications of this finding is that in order to prevent transcription termination, LicT must bind to its *licS*-RAT target before the intrinsic terminator hairpin is able to disrupt the RAT hairpin and preclude LicT binding, and it also needs to remain tightly bound until the RNA polymerase escapes the pausing site. Finally, this model predicts that ultimately, when the LicT/RNA complex dissociates after transcription has resumed past the pause site (or has stopped irreversibly), the RAT hairpin will be readily destroyed by the terminator, and LicT will thus not be able to reassociate with the elongated (or truncated) *licS* transcripts. This will permit the recycling of the antitermination protein and prevent its sequestration on mRNA molecules where it is no longer needed.

Our understanding of the LicT-mediated antitermination process brings further insights into the molecular mechanisms of intrinsic termination and its regulation (Fig. 5). In intrinsic termination, pausing of RNAP at the U-tract where RNA–DNA interactions are the weakest is thought to be the first step and a prerequisite to efficient termination (Peters et al. 2011; Santangelo and Artsimovitch 2011). This event allows time for the intrinsic terminator to fold into a stable RNA hairpin, and for regulator/ribosomes interactions (Herbert et al. 2006; Landick 2006; Weixlbaumer et al. 2013; Ray-Soni et al. 2016). In vivo, the competitive RNA

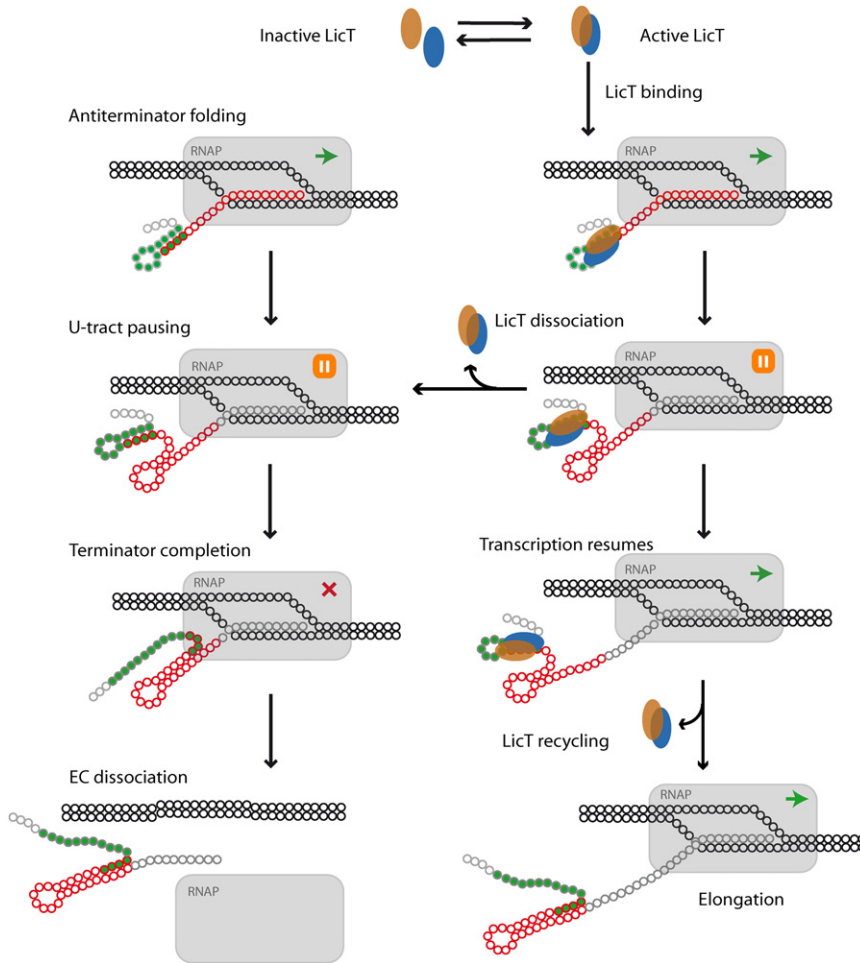


FIGURE 5. Schematic of the kinetic model of LicT-regulated termination–antitermination at the RNAP pausing site. When LicT is monomeric and inactive (*left panel*), the RAT antiterminator hairpin that forms in the 5′UTR of the *licS* gene (in green) is disrupted by the more stable overlapping intrinsic terminator hairpin (in red) that folds during RNAP pausing at the U-tract, leading to RNA release and termination of transcription. When LicT forms an active dimer (*right panel*), it can bind and stabilize the antiterminator hairpin as soon it starts to fold. If LicT remains bound during transcription of the terminator and RNAP pausing, the RAT hairpin remains closed and folding of the terminator hairpin cannot be completed. The polymerase can then escape the termination site to resume transcription of the downstream *licS* gene. If LicT dissociates while the RNAP is still pausing, the terminator forms and disrupts the RAT hairpin. LicT being unable to rebind unfolded RAT, termination occurs at the RNAP pausing site. Ultimately LicT will dissociate from the elongated mRNA, allowing the complete folding of the terminator hairpin and disruption of the LicT binding site, thereby permitting the recycling of the antitermination protein.

folding/unfolding kinetic model proposed above (Fig. 5) is expected to be influenced by many intrinsic and extrinsic factors.

First, the length of the RNA segment separating the 3′ ends of the RAT and the terminator sequences will influence the time available for LicT to bind to its RAT target. This length is 54 nt in the case of the *licS* 5′UTR, and it is interesting to note that in the case of most mRNAs targeted by BglG/SacY family members (Clerte et al. 2013), the length of the terminator sequence is rather long compared to that generally found at the end of natural gene transcripts (Chen et al. 2013).

In a simple model, assuming the same elongation rate, this is giving more time to the antitermination protein to catch and clamp its specific RAT target.

Second, any modulation of the elongation rate will also influence the time window for LicT binding. Indeed, formation of RNA secondary structures in the nascent transcript such as the antiterminator hairpin or nucleation of the partially transcribed terminator may slow down the RNAP or cause elemental pausing (Weixlbaumer et al. 2013; Ray-Soni et al. 2016), in addition to the one observed at the U-tract. Reversible pausing of the elongation complex along the DNA template can last from seconds to minutes depending on sequence determinants and regulatory actors (Lee et al. 1990), whereas many parameters contribute to the strength of intrinsic terminators (Chen et al. 2013). Interestingly, the very long stretch of U’s found at the 3′ end of the *licS* terminator (12 U’s interrupted by a single A at position 6 of the U-tract) usually correlates with a high terminator strength (Chen et al. 2013). Moreover, the first 4 nt of this U-stretch can base pair an AAAA sequence at the terminator 5′ end, and this might further increase termination efficiency by contributing to the ratcheting of the U-tract from the DNA and accelerating the dissociation of the RNA from the paused elongation complex (Chen et al. 2013; Ray-Soni et al. 2016). This A–U-tract pairing is impeded by the stabilization by LicT of the antitermination hairpin, including by direct protein contacts with the AAAA sequence (Fig. 1B).

Finally, it is interesting to note that the affinity between BglG antitermination proteins and their RAT sequence covers a very wide concentration range.

Indeed, dissociation constants at physiological salt concentrations were measured between subnanomolar to >10 μM (Declerck et al. 2002; Hübner et al. 2011; Clerte et al. 2013; this study). Assuming a diffusion-limited RNA-binding kinetic for LicT, this equilibrium constant corresponds to a typical complex half-time of a few milliseconds to minutes. Thus, it appears that once the antitermination protein is bound to its RNA target before the terminator is transcribed (see above), the stability of this complex will ultimately have a strong influence on the fate of the antitermination–termination balance.

In conclusion, we investigated using single-molecule FRET a complex, dynamic RNA termination–antitermination mimic, and have explored some of the molecular determinants that lead to the balance between these mutually exclusive structures, including the stabilization by an antitermination protein. The unveiled molecular mechanism is likely to be globally similar for all BglG/SacY family members, but it could be different in the details, given for example the wide range of stabilities measured for various antiterminator hairpins (Clerte et al. 2013), or of affinities for the antitermination protein/RNA complex (Declerck et al. 2002; Hübner et al. 2011; Clerte et al. 2013). The original approach developed here could be readily adapted, for a better understanding of other riboswitches systems, or help the design of artificial conditional terminators–antiterminators for the control and monitoring of synthetic circuits of gene expression (Chen et al. 2013; Zampini et al. 2016).

MATERIALS AND METHODS

Protein expression and purification

Full-length activated and double-mutant LicT-H207D/H269D (LicT*, 283 residues) (Declerck et al. 2001; van Tilbeurgh et al. 2001) were expressed as an N-terminal His-tag fusion using a pQE30 vector (Qiagen) and purified by affinity chromatography and size exclusion chromatography as previously described (Declerck et al. 1999). Aliquots of the proteins were stored at -80°C in gel-filtration buffer containing 10 mM Tris, pH 8, 0.2 mM EDTA, 2 mM DTT, and 300 mM NaCl. Before use, aliquots were clarified by centrifugation and the protein concentration was determined by OD measurements at 280 nm using a NanoDrop (Thermo Fisher) spectrophotometer.

Nucleic acids preparation

Atto647N-labeled *licS* RNA, terminator mimic oligonucleotides (*T* to *TΔ6*), and *DNAc* labeled with Cy3B were purchased from IBA GmbH. The quality of the oligonucleotides and their lack of degradation were checked by PAGE analysis (Supplemental Fig. S1B). The DNA oligonucleotide *Opener* was purchased from Eurogentec. Hybridization was performed by heating the various complementary RNA/DNA strands and *licS* RNA at 95°C at 100 nM in buffer Y (20 mM HEPES, pH 7.5, 0.1 mM EDTA, 150 mM KAc) and slowly cooling down using a thermocycler apparatus. RNA hybrids were stored at -20°C and diluted in reaction buffer before use.

Gel mobility shift experiments

LicT* was mixed with the RNA hybrids (at final concentrations as indicated in figure legends). After 10 min at room temperature, the mix was rapidly loaded onto 8% polyacrylamide gel (acrylamide/bisacrylamide, 19:1, w/w) immersed in ice-cold $0.5\times$ TBE buffer. The electrophoresis was run for ~ 1 h at 150 V. The fluorescent signal was detected by using a Carestream Image Station.

Fluorescence anisotropy assays

Fluorescence anisotropy titrations were performed in Corning NBS 384-well plates by adding 40 μL of Atto647N-labeled *licS* RAT (0.4 nM) to 40 μL of serial dilutions of purified LicT*. Fluorescence polarization was measured at 25°C using a Tecan Sapphire II plate reader, with the excitation wavelength set at 630 nm and the emission at 680 ± 10 nm. Buffer conditions were 10 mM Tris–HCl (pH 8), 1 mM EDTA, 1 mM DTT, 75 $\mu\text{g}/\text{mL}$ BSA, and 150 mM NaCl.

smFRET coupled to pulsed interleaved excitation (PIE)

smFRET experiments with PIE configuration were performed on a homemade confocal microscope as previously described (Olofsson and Margeat 2013). A pulsed supercontinuum laser source (SC450-4-20MHz, Fianium) was divided into two beams spectrally filtered at the desired wavelengths (532 nm [prompt beam] and 635 nm [optically delayed by 25 nsec]). The two beams were recombined, interleaved, and coupled into a single-mode fiber (SMF) (P1-460A-FC, Thorlabs). The output beams were collimated using a $10\times$ objective, polarized via a polarizing beamsplitter and focused using a Nikon $100\times$, 1.4 NA objective to define a confocal femtoliter volume where highly diluted (10 pM) diffusing fluorescently labeled molecules are excited. Emitted photons were then collected by the objective, focused on a pinhole (150 μm), divided into their parallel and perpendicular components via a polarizing beamsplitter. In each created channel, the photons were then spectrally separated using dichroic mirrors (BS 649, Semrock) and filtered using high quality emission bandpass filters (ET BP 585/65 and ET BP 700/75, Chroma). Single photons were detected using Single Photon Avalanche Diodes. We used two MPD-1CTC (MPD) for the lowest wavelength channels and two SPCM AQR-14 (PerkinElmer) for the highest wavelength channels. Photons were collected using a time-correlated single-photon counting (TCSPC) board (SPC-150, Becker & Hickl). Data were analyzed with the Software Package for Multiparameter Fluorescence Spectroscopy, Full Correlation and Multiparameter Fluorescence Imaging developed in the C.A.M. Seidel laboratory (Widengren et al. 2006) (www.mpc.uni-duesseldorf.de). The proximity ratio E_{PR} that reports on the proximity between the donor (D) and the acceptor (A) is defined as follows:

$$E_{\text{PR}} = \frac{F_{\text{GR}}}{F_{\text{GR}} + F_{\text{GG}}},$$

where F_{GG} and F_{GR} are the total fluorescence intensity in all green and all red detection channels, respectively, after green excitation. Experimental histograms obtained only for molecules containing a donor and an acceptor (thanks to the PIE/ALEX scheme [Kapanidis et al. 2004]) are displayed and fitted using Origin. The single-molecule buffer (SMB) for all measurements was 10 mM Tris (pH 8), 150 mM NaCl, 1 mM EDTA, 1 mM DTT, and BSA 75 $\mu\text{g}/\text{mL}$.

SUPPLEMENTAL MATERIAL

Supplemental material is available for this article.

ACKNOWLEDGMENTS

This article is dedicated to the memory of Michel Kochoyan, our colleague and partner, who passed away on May 16, 2016. This work was supported by the French National Research Agency (ANR 2010 BLAN 1525 01 to E.M.); a “Chercheur d’Avenir” grant from the Region Languedoc Roussillon to E.M.; a post-doctoral grant from the Université de Montpellier to S.A.-B.; the France-BioImaging infrastructure supported by the French National Research Agency (ANR-10-INBS-04, “Investments for the future”); and the GIS “IBISA: Infrastructures en Biologie Sante et Agronomie.”

Received December 16, 2016; accepted February 8, 2017.

REFERENCES

- Ait-bara S, Clerté C, Margeat E. 2015. Single-molecule FRET characterization of RNA remodeling induced by an antitermination protein. *Methods Mol Biol* **1259**: 349–368.
- Amster-Choder O. 2005. The *bgl* sensory system: a transmembrane signaling pathway controlling transcriptional antitermination. *Curr Opin Microbiol* **8**: 127–134.
- Aymerich S, Steinmetz M. 1992. Specificity determinants and structural features in the RNA target of the bacterial antiterminator proteins of the BglG/SacY family. *Proc Natl Acad Sci* **89**: 10410–10414.
- Chen Y, Liu P, Nielsen AAK, Brophy JAN, Clancy K, Peterson T, Voigt CA. 2013. Characterization of 582 natural and synthetic terminators and quantification of their design constraints. *Nat Methods* **10**: 659–664.
- Clerte C, Declerck N, Margeat E. 2013. Competitive folding of anti-terminator/terminator hairpins monitored by single molecule FRET. *Nucleic Acids Res* **41**: 2632–2643.
- Daguer JP, Geissmann T, Petit-Glatron MF, Chambert R. 2004. Autogenous modulation of the *Bacillus subtilis* *sacB-levB-yveA* levan-sucrase operon by the *levB* transcript. *Microbiology* **150**: 3669–3679.
- Declerck N, Vincent F, Hoh F, Aymerich S, van Tilbeurgh H. 1999. RNA recognition by transcriptional antiterminators of the BglG/SacY family: functional and structural comparison of the CAT domain from SacY and LicT. *J Mol Biol* **294**: 389–402.
- Declerck N, Dutartre H, Receveur V, Dubois V, Royer C, Aymerich S, van Tilbeurgh H. 2001. Dimer stabilization upon activation of the transcriptional antiterminator LicT. *J Mol Biol* **314**: 671–681.
- Declerck N, Minh NL, Yang Y, Bloch V, Kochoyan M, Aymerich S. 2002. RNA recognition by transcriptional antiterminators of the BglG/SacY family: mapping of SacY RNA binding site. *J Mol Biol* **319**: 1035–1048.
- Déméné H, Ducat T, De Guillen K, Birck C, Aymerich S, Kochoyan M, Declerck N. 2008. Structural mechanism of signal transduction between the RNA-binding domain and the phosphotransferase system regulation domain of the LicT antiterminator. *J Biol Chem* **283**: 30838–30849.
- Deutscher J, Francke C, Postma PW. 2006. How phosphotransferase system-related protein phosphorylation regulates carbohydrate metabolism in bacteria. *Microbiol Mol Biol Rev* **70**: 939–1031.
- Gordon N, Rosenblum R, Nussbaum-Shochat A, Eliahou E, Amster-Choder O. 2015. A search for ribonucleic antiterminator sites in bacterial genomes: not only antitermination? *J Mol Microbiol Biotechnol* **25**: 143–153.
- Graille M, Zhou CZ, Receveur-Bréchet V, Collinet B, Declerck N, van Tilbeurgh H. 2005. Activation of the LicT transcriptional antiterminator involves a domain swing/lock mechanism provoking massive structural changes. *J Biol Chem* **280**: 14780–14789.
- Gusarov I, Nudler E. 1999. The mechanism of intrinsic transcription termination. *Mol Cell* **3**: 495–504.
- Hendrix J, Lamb DC. 2013. Pulsed interleaved excitation: principles and applications. *Methods Enzymol* **518**: 205–243.
- Herbert KM, La Porta A, Wong BJ, Mooney RA, Neuman KC, Landick R, Block SM. 2006. Sequence-resolved detection of pausing by single RNA polymerase molecules. *Cell* **125**: 1083–1094.
- Heyduk T, Ma Y, Tang H, Ebricht RH. 1996. Fluorescence anisotropy: rapid, quantitative assay for protein-DNA and protein-protein interaction. *Methods Enzymol* **274**: 492–503.
- Himmel S, Zschiedrich CP, Becker S, Hsiao HH, Wolff S, Diethmaier C, Urlaub H, Lee D, Griesinger C, Stülke J. 2012. Determinants of interaction specificity of the *Bacillus subtilis* GlcT antitermination protein: functionality and phosphorylation specificity depend on the arrangement of the regulatory domains. *J Biol Chem* **287**: 27731–27742.
- Hübner S, Declerck N, Diethmaier C, Le Coq D, Aymerich S, Stülke J. 2011. Prevention of cross-talk in conserved regulatory systems: identification of specificity determinants in RNA-binding antitermination proteins of the BglG family. *Nucleic Acids Res* **39**: 4360–4372.
- Joyet P, Bouraoui H, Aké FMD, Derkaoui M, Zébré AC, Cao TN, Ventroux M, Nessler S, Noiroi-Gros MF, Deutscher J, et al. 2013. Transcription regulators controlled by interaction with enzyme IIB components of the phosphoenolpyruvate:sugar phosphotransferase system. *Biochim Biophys Acta* **1834**: 1415–1424.
- Kapanidis AN, Lee NK, Laurence TA, Dooze S, Margeat E, Weiss S. 2004. Fluorescence-aided molecule sorting: analysis of structure and interactions by alternating-laser excitation of single molecules. *Proc Natl Acad Sci* **101**: 8936–8941.
- Krüger S, Hecker M. 1995. Regulation of the putative *bglPH* operon for aryl- β -glucoside utilization in *Bacillus subtilis*. *J Bacteriol* **177**: 5590–5597.
- Landick R. 2006. The regulatory roles and mechanism of transcriptional pausing. *Biochem Soc Trans* **34**: 1062–1066.
- Le Coq D, Lindner C, Krüger S, Steinmetz M, Stülke J. 1995. New β -glucoside (*bgl*) genes in *Bacillus subtilis*: the *bglP* gene product has both transporter and regulatory functions similar to those of BglF, its *Escherichia coli* homolog. *J Bacteriol* **177**: 1527–1535.
- Lee DN, Phung L, Stewart J, Landick R. 1990. Transcription pausing by *Escherichia coli* RNA polymerase is modulated by downstream DNA sequences. *J Biol Chem* **265**: 15145–15153.
- Lindner C, Galinier A, Hecker M, Deutscher J. 1999. Regulation of the activity of the *Bacillus subtilis* antiterminator LicT by multiple PEP-dependent, enzyme I- and HPr-catalysed phosphorylation. *Mol Microbiol* **31**: 995–1006.
- Mahadevan S, Wright A. 1987. A bacterial gene involved in transcription antitermination: regulation at a rho-independent terminator in the *bgl* operon of *E. coli*. *Cell* **50**: 485–494.
- Manival X, Yang Y, Strub MP, Kochoyan M, Steinmetz M, Aymerich S. 1997. From genetic to structural characterization of a new class of RNA-binding domain within the SacY/BglG family of antiterminator proteins. *EMBO J* **16**: 5019–5029.
- Naville M, Gautheret D. 2010. Briefings in functional genomics transcription attenuation in bacteria. *Brief Funct Genomic Proteomic* **9**: 178–189.
- Olofsson L, Margeat E. 2013. Pulsed interleaved excitation fluorescence spectroscopy with a supercontinuum source. *Opt Express* **21**: 3370–3378.
- Peters JM, Vangeloff AD, Landick R. 2011. Bacterial transcription terminators: the RNA 3'-end chronicles. *J Mol Biol* **412**: 793–813.
- Ray-Soni A, Bellecourt MJ, Landick R. 2016. Mechanisms of bacterial transcription termination: all good things must end. *Annu Rev Biochem* **85**: 319–347.
- Santangelo TJ, Artsimovitch I. 2011. Termination and antitermination: RNA polymerase runs a stop sign. *Nat Rev Microbiol* **9**: 319–329.
- Schnetzer K, Stülke J, Gertz S, Krüger S, Krieg M, Hecker M, Rak B. 1996. LicT, a *Bacillus subtilis* transcriptional antiterminator protein of the BglG family. *J Bacteriol* **178**: 1971–1979.
- Smith AM, Fuchs RT, Grundy FJ, Henkin TM. 2010. Riboswitch RNAs: regulation of gene expression by direct monitoring of a physiological signal. *RNA Biol* **7**: 104–110.

- Steinmetz M, Aymerich S. 1986. [Genetic analysis of *sacR*, a *cis*-regulator of levan-saccharase synthesis of *Bacillus subtilis*]. *Ann Inst Pasteur Microbiol* **137A**: 3–14.
- Stülke J, Arnaud M, Rapoport G, Martin-Verstraete I. 1998. PRD—a protein domain involved in PTS-dependent induction and carbon catabolite repression of catabolic operons in bacteria. *Mol Microbiol* **28**: 865–874.
- Tortosa P, Le Coq D. 1995. A ribonucleic antiterminator sequence (RAT) and a distant palindrome are both involved in sucrose induction of the *Bacillus subtilis* *sacXY* regulatory operon. *Microbiology* **141**: 2921–2927.
- Tortosa P, Declerck N, Dutartre H, Lindner C, Deutscher J, Le Coq D. 2001. Sites of positive and negative regulation in the *Bacillus subtilis* antiterminators LicT and SacY. *Mol Microbiol* **41**: 1381–1393.
- van Tilbeurgh H, Declerck N. 2001. Structural insights into the regulation of bacterial signalling proteins containing PRDs. *Curr Opin Struct Biol* **11**: 685–693.
- van Tilbeurgh H, Le Coq D, Declerck N. 2001. Crystal structure of an activated form of the PTS regulation domain from the LicT transcriptional antiterminator. *EMBO J* **20**: 3789–3799.
- Weiss S. 2000. Measuring conformational dynamics of biomolecules by single molecule fluorescence spectroscopy. *Nat Struct Biol* **7**: 724–729.
- Weixlbaumer A, Leon K, Landick R, Darst SA. 2013. Structural basis of transcriptional pausing in bacteria. *Cell* **152**: 431–441.
- Widengren J, Kudryavtsev V, Antonik M, Berger S, Gerken M, Seidel CAM. 2006. Single-molecule detection and identification of multiple species by multiparameter fluorescence detection. *Anal Chem* **78**: 2039–2050.
- Xayaphoummine A, Bucher T, Isambert H. 2005. Kinefold web server for RNA/DNA folding path and structure prediction including pseudoknots and knots. *Nucleic Acids Res* **33**: W605–W610.
- Yang Y, Declerck N, Manival X, Aymerich S, Kochoyan M. 2002. Solution structure of the LicT-RNA antitermination complex: CAT clamping RAT. *EMBO J* **21**: 1987–1997.
- Zampini M, Mur LAJ, Rees Stevens P, Pachebat JA, Newbold CJ, Hayes F, Kingston-Smith A. 2016. Terminator Operon Reporter: combining a transcription termination switch with reporter technology for improved gene synthesis and synthetic biology applications. *Sci Rep* **6**: 26572.